Jamming as a Multicritical Point

Danilo B. Liarte,[1,*] Xiaoming Mao,[2] Olaf Stenull,[3] and T. C. Lubensky[3,†]
[1]Laboratory of Atomic and Solid State Physics, Cornell University, Ithaca, New York 14853, USA
[2]Department of Physics, University of Michigan, Ann Arbor, Michigan 40109, USA
[3]Department of Physics and Astronomy, University of Pennsylvania, Philadelphia, Pennsylvania 19104, USA

(Received 25 September 2018; published 28 March 2019)

The discontinuous jump in the bulk modulus B at the jamming transition is a consequence of the formation of a critical contact network of spheres that resists compression. We introduce lattice models with underlying undercoordinated compression-resistant spring lattices to which next-nearest-neighbor springs can be added. In these models, the jamming transition emerges as a kind of multicritical point terminating a line of rigidity-percolation transitions. Replacing the undercoordinated lattices with the critical network at jamming yields a faithful description of jamming and its relation to rigidity percolation.

DOI: 10.1103/PhysRevLett.122.128006

Jamming [1,2] is now well established as a phenomenon with a zero-temperature mechanical critical point that separates a state of free particles from one in which they collectively resist elastic distortions. The jamming critical point (J) is, however, unusual in that it exhibits properties of both a first-order transition (with a discontinuous jump in the bulk modulus, B) and a second-order one (with a continuous growth of the shear moduli, G, from zero). This is in stark contrast to its cousin, the rigidity-percolation (RP) transition [3,4], in which both the bulk and shear moduli grow linearly from zero above the RP critical point (or line). The first-order jump in B is a consequence of the formation of a critical network of contacts that resists compression. This fact is the inspiration for our introduction of lattice models with sublattices that also resist compression. In our analysis of these models using the effective medium theory (EMT) [3,5] and numerical simulations, the jamming transition corresponds to a kind of multicritical point at which a line (or surface) of RP transitions meets a line along which B is nonzero.

Our models begin with the undercoordinated honeycomb lattice in two dimensions (2D) or the diamond lattice in 3D, each consisting of sites connected by nearest-neighbor (NN) springs, with a nonvanishing bulk modulus but with vanishing shear moduli [6]. Next-nearest-neighbor (NNN) springs are randomly added [as shown in Fig. 1(a)], leading to the phase diagrams shown in Figs. 1(b)–1(e). At a critical concentration of NNN springs, the Maxwell rigidity criterion [7] is reached, the shear modulus begins to grow continuously from zero, and the bulk modulus begins to increase. This model mimics important aspects of jamming and the jamming transition, which is reached by increasing the volume fraction of spheres until they have a sufficient number of contacts to first resist compression, indicating a bulk modulus that is greater than zero. The marginally jammed state that is formed is an analog of the honeycomb or diamond lattice in our model. Further compression of the jammed lattice increases the number of contacts and produces an increase in the shear moduli from zero. This is the analog of adding NNN bonds in our models.

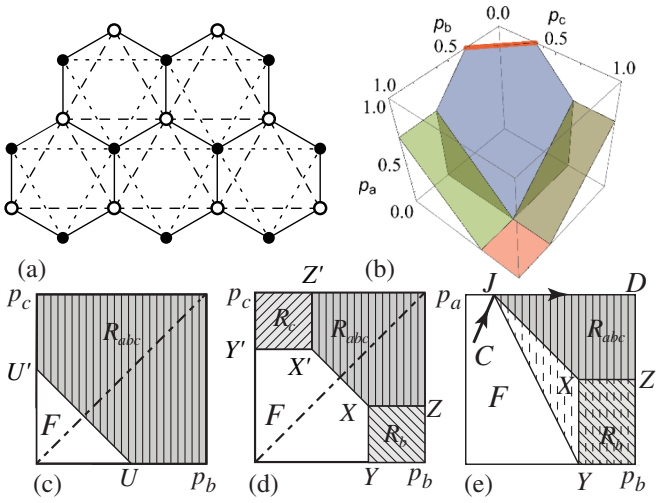

FIG. 1. (a) Three-sublattice model showing NN (solid lines) and NNN (dashed and dotted lines) bonds, the latter of which connect sites in either of the triangular sublattices containing the first (black) or second (open) sites of the honeycomb lattice. (b) 3D phase diagram showing the surfaces S_{FRabc} (blue), S_{RbRabc} (green), S_{RcRabc} (khaki), S_{FRb} (dark green), and S_{FRc} (dark khaki) and the jamming line L_J (red); (c)–(e) 2D slices of the 3D diagram at (c) constant $2/3 < p_a < 1$, (d) constant $0 < p_a < 2/3$, and (e) both $p_c = 1/6$ at $p_b = p_c$, showing the F, R_b, R_c, and R_{abc} phases. UU' is the jamming line when $p_a = 1$ and an RP line when $p_a < 1$. XX', XY, $X'Y'$, JX, and JY are RP lines, and XZ marks the transition from the R_b to the R_{abc} phase. In (e), the region to the right of JX is the R_{abc} phase when $p_a = p_b$, and the line JX is not a part of the figure when $p_c = 1/6$. CJD is a jamming path with a discontinuous jump in B.

Our model differs from jamming in that sites in the former are fixed on a periodic lattice whereas those in the latter are off lattice and change positions with compression. In addition, the bulk modulus in our models remains nonzero below the jamming transition as long as the NN bonds are occupied with unit probability. Our approach, however, can be applied to any lattice that has an under- or critically coordinated sublattice with nonzero B, such as that discussed at the end of this Letter and in Supplemental Material [8].

Our model exploits the fact that both the honeycomb and the diamond lattices with NNN bonds can be divided into three independent bond lattices, each sharing the sites of the original NN lattice: the original NN lattice (the a lattice) and two independent NNN lattices (the b and c lattices) with sites, respectively, on one or the other site sublattices of the a lattice [see Fig. 1(a)]. Population of the bonds of these lattices with springs of spring constant k with probabilities p_a, p_b, and p_c gives rise to EMT spring constants k_a, k_b, and k_c, respectively. In what follows, we will focus on the 2D case, though most of the results we present apply to the diamond lattice as well.

The full 3D EMT phase diagram, depicted in Fig. 1(b), in the space defined by (p_a, p_b, p_c) shows four distinct phases: a floppy phase F, in which B and G are zero at zero frequency, and three rigid phases with $B > 0$ and $G > 0$: R_b, in which only $k_b > 0$; R_c, in which only $k_c > 0$; and R_{abc}, in which k_a, k_b, and k_c are all nonzero. In addition, it shows boundary surfaces S_{AB} where phases A and B meet, lines L_{ABC} where phases A, B, and C meet, and the jamming line L_J (in red) where S_{FRabc} meets the plane $p_a = 1$. Figures 1(c)–1(e) depict various 2D slices. In Fig. 1(c), the line $U'U$ is L_J when $p_a = 1$. In Fig. 1(e), J is the point on L_J when $p_c = 1/6$. Surfaces S_{FR} for R equal to R_b, R_c, or R_{abc} and lines XY, XX', $Y'X'$, JX, and JY correspond to RP transitions, and surfaces S_{RRabc}, with $R = R_b$ or R_c, and line XZ represent transitions in which k_a develops a nonzero value when k_b or k_c is already nonzero. In Fig. 1(e), J, viewed from the F phase, is a critical end point [9] where the second-order RP line JY meets the first-order line at $p_a = 1$. In what follows, we will focus on the vicinity of the points J and X in the 2D slices.

As shown in previous studies (see, e.g., [3,10,11]), the EMT provides accurate but not exact estimates of elastic moduli and phase boundaries. In particular, it does not incorporate redundant bonds [11] that lead to over- and underconstrained regions in randomly diluted samples. Our results agree with this previous work (see Fig. 2): Simulations and EMT track each other closely, but with larger deviations near rigidity transitions and particularly near point X where simulations do not show discontinuous slope changes predicted by the EMT (see Supplemental Material [8]).

In Fig. 1(e), k_a, and thus B, is nonzero along the line $p_a = 1$, but k_b and k_c are (for both $p_b = p_c$ and $p_c = 1/6$)

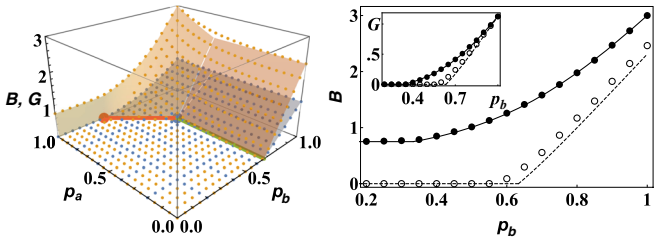

FIG. 2. Left: Simulations (points) and EMT solutions (surfaces) for B (yellow) and G (blue) as a function of p_a and p_b for $p_c = 0$. Red and green lines correspond to JX and XY in Fig. 1(e), respectively. Right: B and G (inset) as a function of p_b from EMT (lines) and simulations (circles) for $p_c = 0$ and $p_a = 1$ (filled circles) and $p_a = 0.7$ (open circles).

zero along this line for p_b less than or equal to its value p_b^J at J. Thus, G but not B approaches zero as J is approached along not only the line $p_a = 1$, but along any line approaching J from the rigid side. On the other hand, if J is approached from the floppy side along any path [e.g., CJD in Fig. 1(e)] other than $p_a = 1$, B will undergo a discontinuous change at L_J as in jamming. We argue that a path with $p_a < 1$ until J is reached followed by a path along $p_a = 1$ for $p_b > p_b^J$ faithfully represents the jamming transition. If springs are removed randomly from a jammed lattice at J, it immediately loses its rigidity. This also takes place in our model if we allow the removal of springs from the a lattice as well as the b and c lattices, i.e., follow a path in F in which $p_a < 1$ until L_J is reached. The jamming line at $p_a = 1$ terminates an RP surface (S_{FRabc}) across which all effective spring constants, and thus both B and G, grow linearly with distance from it.

EMTs also yield information about finite frequency behavior [5,12–18] with the inclusion of inertia of mass points and/or viscous friction with a background fluid [19]. In our case, the former yields densities of states that scale like those near jamming, and the latter lead to renormalized shear and bulk viscosities in the floppy regime, the former of which diverge as $|\Delta\tilde{p}|^{-1}$ at the S_{RP}'s and along L_J, and the latter of which also diverge as $|\Delta\tilde{p}|^{-1}$ at the S_{RP}'s but as $|\Delta\tilde{p}|^{-2}$ along paths terminating at L_J.

Our EMT replaces randomly placed springs with spring constant $k = 1$ in the three lattices with homogeneously placed ones with respective effective spring constants k_a, k_b, and k_c such that the average scattering from any given spring in the effective background medium is zero. The EMT equations are then

$$k_\alpha(\omega) = [p_\alpha - h_\alpha(\omega)]/[1 - h_\alpha(\omega)], \qquad \alpha = a, b, c, \quad (1)$$

$$h_\alpha(\omega) = \frac{1}{\tilde{z}_\alpha N_c} \sum_{\mathbf{q}} \mathrm{Tr} k_\alpha(\omega) K_\alpha(\mathbf{q}) \mathcal{G}(\mathbf{q}, \omega), \quad (2)$$

where $\mathcal{G}(\mathbf{q}, \omega) = [\sum_\beta k_\beta(\omega) K_\beta(\mathbf{q}) - w(\omega) I]^{-1}$ is the lattice Green's function, N_c the number of unit cells, $\tilde{z}_\alpha$ (=3 for all

α in the honeycomb lattice) the number of bonds per unit cell in lattice α ($= a, b, c$), $K_\alpha(\mathbf{q})$ the α-lattice normalized stiffness matrix, and $w(\omega) = \omega^2 + i\gamma\omega$, where ω is the frequency, γ is the drag coefficient, and the mass is set to one. As discussed in Supplemental Material [8], the evaluation of h_α in the limit where k_b, k_c, and w tend to zero requires some care, because K_a has a zero eigenvalue at every $\mathbf{q}$. The $k_\alpha(\omega)$ are determined by the self-consistent solution to Eqs. (1) and (2). In the zero-frequency limit $[w(\omega) \to 0]$, $k_\alpha \equiv k_\alpha(\omega = 0) = 0$ when $p_\alpha = h_\alpha(\omega = 0) \equiv h_\alpha$, $k_\alpha = 1$ when $p_\alpha = 1$, and $0 \le k_\alpha \le 1$ for $h_\alpha \le p_\alpha \le 1$. As we shall see, k_α vanishes as $w(\omega) \to 0$ when $p_\alpha < h_\alpha$.

It follows from Eq. (2) that the h_α's satisfy the sum rule

$$\sum_\alpha \tilde{z}_\alpha h_\alpha(\omega) = mD + [w(q)/N_c] \sum \mathrm{Tr}\mathcal{G}(\boldsymbol{q}, \omega), \quad (3)$$

where D is the spatial dimension and $m = 2$ is the number of sites per unit cell in the honeycomb and diamond lattices. Equation (3) along with the results of Eq. (1) that $h_\alpha = p_\alpha$ when $k_\alpha = 0$ yield the Maxwell condition for marginal stability on the S_{FRabc} surface or on the jamming line at $\omega = 0$:

$$\tilde{z}_a p_a + \tilde{z}_b (p_b + p_c) = mD. \quad (4)$$

The surfaces S_{FRb} and S_{FRc} signal the onset of rigidity of the b and c lattices individually, in which case k_a and k_b (k_c) adopt the vanishing solutions to Eq. (2). In this case, the rigid b (c) lattice is triangular and has only one site per unit cell, and $h_b = D/\tilde{z}_b = 2/3$ throughout the R_b phase, and similarly for h_c. At S_{RbRabc}, k_a and k_c first adopt nonzero solutions to Eqs. (2) and (1), and $h_a = p_a$ and $h_c = p_c$ to yield $\tilde{z}_a p_a + \tilde{z}_b p_c = (m-1)D$ on S_{RbRabc}.

We will now focus on critical points and lines in Figs. 1(d) and 1(e). As noted above, J marks the jamming point and X the critical point where F, R_{abc}, and R_b meet. At fixed p_c, $J = (1, p_b^J, p_c)$, where $p_b^J = (1/3) - p_c$, and $X = (2/3 - p_c, 2/3, p_c)$ (for $0 < p_c < 2/3$). At $p_b = p_c$, $J = (1, 1/6, 1/6)$ and $X = (1/2, 2/3, 1/6)$. Figure 1(e) shows phase-diagram slices for $p_c = 1/6$ and for $p_b = p_c$. The lines JX and JY satisfy the equation

$$\Delta\tilde{p} \equiv \Delta p_b^J - \nu \Delta p_a^J = 0, \quad (5)$$

where $\Delta p_b^J = p_b - p_b^J$, $\Delta p_a^J = (1 - p_a) > 0$, and the inverse slope is $\nu = \nu_X = 1$ for the line JX at fixed $p_c = 1/6$ and $\nu = \nu_Y = 1/2$ for the line JY and $p_c = p_b$.

Along the $F - R_{abc}$ lines JX or JY, all effective spring constants (on bonds with nonzero occupation probability), and thus all elastic moduli, grow linearly with $\Delta\tilde{p}$, and along the $F - R_b$ line, k_b grows linearly with $\Delta p_b = p_b - 2/3$:

$$k_r^{JV} = c_r^{JV}[\Delta\tilde{p}], \qquad k_b^{XY} = c_b^{XY}[\Delta p_b], \quad (6)$$

where $[\phi] = (\phi + |\phi|)/2$, $r = a, b$, $V = X, Y$, and c_r^{JV} varies with position along JV. Along the line $p_a = 1$, k_a is exactly equal to one. Near J, k_b maintains its form of Eq. (6), but k_a has to vanish on JV and equal one at $p_a = 1$. This is accomplished within the EMT by

$$k_b^J = \frac{[\Delta\tilde{p}]}{s + \nu c_J}; \qquad k_a^J = \frac{c_J k_B^J}{c_J k_B^J + \Delta p_a^J} \to \frac{c_J \Delta\tilde{p}}{c_J \Delta p_b^J + s \Delta p_a^J}, \quad (7)$$

where $s = 1 - p_b^J$. When $\Delta p_a^J = 0$, $k_a^J = 1$ as required. Also, k_a^J clearly vanishes along JV where $\Delta\tilde{p} = 0$. The elastic moduli of the honeycomb lattice in terms of the k's are $G = r_b k_b + r_c k_c$ and $B = s_a k_a + s_b k_b + s_c k_c$, where $r_b = r_c = 9/8$, $s_a = 3/4$, $s_b = s_c = 9/4$, and as advertised, G vanishes linearly with $\Delta\tilde{p}$. The value of k_a and thus of B depends on the path to the jamming point as can be seen by putting $\Delta p_b^J = \nu' \Delta p_a^J$ in Eq. (7) with $\nu' > \nu$: $k_a^J = c_J(\nu' - \nu)/(c_J \nu' + s)$. The ratio G/B approaches zero, and the Poisson ratio σ approaches its limit value of one along all paths to J. G/B reaches a value along the RP line JY increasing from zero at J to a maximum of $1/2$ at Y. These results are similar to those in Refs. [20,21].

We now turn to behavior in the vicinity of X. The EMT solution at $w = 0$ is

$$k_b^X = [\Delta\tilde{p}_{ab}^X]/s_b \quad \text{and} \quad k_a^X = k_b^X [\Delta p_a^X]/c_X, \quad (8)$$

where $\Delta\tilde{p}_{ab}^X = \Delta p_b^X + \nu_X [\Delta p_a^X]$, $\Delta p_b^X = p_b - p_b^X$, $\Delta p_a^X = p_a - p_a^X$, $c_X \approx 0.1$ (evaluated numerically), and $s_b = 1 - p_b^X$. These equations encode all of the phase boundaries incident at X: $\Delta\tilde{p}_{ab}^X$ is equal to Δp_b^X when $\Delta p_a^X < 0$ and to $\Delta\tilde{p}^X = \Delta p_b^X + \nu_X \Delta p_a^X$ when $\Delta p_a^X > 0$ so that $k_b^X = 0$ for $\Delta p_a^X < 0$ and $\Delta p_b^X < 0$ and for $\Delta\tilde{p}^X < 0$ and $\Delta p_a^X > 0$. The result is that $k_b^X > 0$ in the R_b and R_{abc} phases in Fig. 1 and that k_a^X is nonzero only in the R_{abc} phases of that figure. We have calculated the bulk and shear moduli by numerical solution of the EMT equations for the k_α's and by their direct evaluation on our random lattices. The two solutions are nearly identical over most of phase space as seen in Fig. 2. The simulations, however, do not show the sharp changes near X that the EMT does.

Equation (2) provides dynamical as well as static information, allowing us to calculate the frequency-dependent effective spring constants in the floppy region. Of particular interest is the approach to the jamming point. In the case of $p_b = p_c$, the results (in agreement with Ref. [19] for k_b) are

$$k_b = \frac{1}{2(s + \nu c)} \left[\Delta\tilde{p} + \sqrt{|\Delta\tilde{p}|^2 - 4(s + \nu c_J) v_b w(\omega)} \right] \quad (9)$$

$$\approx \frac{[\Delta\tilde{p}]}{s + \nu c_J} - \frac{v_b w}{|\Delta\tilde{p}|}, \quad \text{when } \frac{v_b w}{|\Delta\tilde{p}|^2} \ll 1, \quad (10)$$

and

$$k_a = \frac{k_b}{k_b + (\Delta p_a^J / c_J)} \tag{11}$$

$$\xrightarrow{\Delta\tilde{p}<0} \frac{v_b w}{v_b w + (\Delta p_a^J |\Delta\tilde{p}|/c)} \approx \frac{c_J v_b w}{\Delta p_a^J |\Delta\tilde{p}|}. \tag{12}$$

Thus, on paths approaching J in the low-frequency limit when $w = i\gamma\omega$, k_b diverges as $|i\gamma\omega\Delta\tilde{p}|^{-1}$, but k_a diverges as $i\gamma\omega|\Delta p_a^J \Delta\tilde{p}|^{-1}$, implying that the shear viscosity diverges as $|\Delta\tilde{p}|^{-1}$, but the bulk modulus viscosity diverges as $|\Delta\tilde{p}|^{-2}$. The scaling of k_b [Fig. 3(a)] is consistent with results for the shear modulus of soft sphere packings near jamming [22]. When $\gamma = 0$ and $w = \omega^2$, our calculations yield a density of states that is nearly constant at small ω [Fig. 3(b)], down to a crossover frequency ω^* that scales as $\Delta\tilde{p}$ (see the inset), as in jamming [23,24].

As noted earlier, in our model, k_a, and thus B, is nonzero in the floppy region when $p_a = 1$. In the jamming protocol, B is zero in the floppy phase and jumps discontinuously at J with the formation of a random marginally stable lattice with a single state of self-stress [25,26] that resists increase in pressure. As volume fraction is increased, more links form, inviting us to model jamming starting with the lattice at J, which is now critically rather than undercoordinated with $\tilde{z}_a = D$ ($\tilde{z}_a$ is half the coordination number), as the analog of the a lattice and identifying "unoccupied bonds" between pairs of close but not touching spheres as the b lattice. Ideally, this b lattice would contain a sufficient number of bonds that it would by itself be mechanically stable if all of these bonds were occupied with springs. We can now use the random-lattice EMT of Refs. [12,13,18], modified to treat lattices a and b separately. The result is a phase diagram (see Supplemental Material [8]) in the $p_a - p_b$ space identical to that in Fig. 1(e) but with the point J moved to the upper left-hand corner: $J = (1, 0)$ and the point Y moved to $Y = (0, D/\tilde{z}_b)$. The path to jamming, which involves first the creation of lattice a, is thus along the line $p_b = 0$ until J is reached. As more springs are added, the path follows the line $p_a = 1$. Of course, different paths can be followed, most of which will intersect the RP line $J - Y$ [3,21]. For example, all paths starting from a point in the jammed phase along $p_a = 1$ in which springs are randomly removed from both a and b sublattices cross the RP line. The EMT equations are identical in form to Eqs. (2) and (1), but with only two sublattices and Eq. (4) replaced by $\tilde{z}_a p_a + \tilde{z}_b p_b = D$, where $\tilde{z}_a = D$. Near J, k_a and k_b obey Eqs. (6), (7), and (12) to (9) with $p_b^J = 0$ and $s = 1$. See Supplemental Material [8] for more detail.

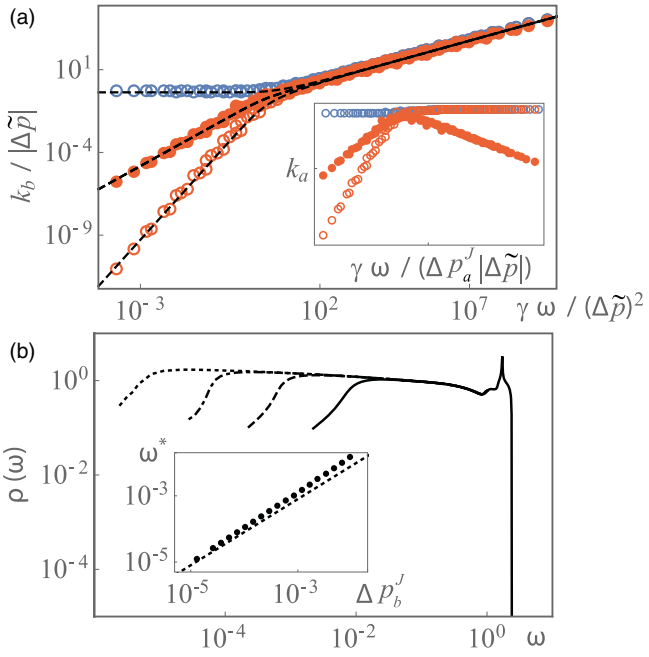

FIG. 3. (a) $k_b/|\Delta\tilde{p}|$ as a function of $\gamma\omega/|\Delta\tilde{p}|^2$ in the low-frequency limit $w = i\gamma\omega$. Blue (red) circles: Numerical solutions to full EMT equations for approach to jamming in the rigid (floppy) phase; black dashed line: asymptotic solutions [Eq. (9)] near jamming critical point; hollow circles: $\mathrm{Re}k_b/|\Delta\tilde{p}|$; filled circles: $-\mathrm{Im}k_b/|\Delta\tilde{p}|$, which is independent of the sign of $|\Delta\tilde{p}|$. Inset: k_a as a function of $\gamma\omega/(\Delta p_a^J|\Delta\tilde{p}|)$. (b) Density of states $\rho(\omega)$ for $p_a = 1$ and $\Delta\tilde{p} = \Delta p_b^J = 10^{-2}$ (solid lines), 10^{-3} (dashed line), 10^{-4} (dot-dashed line), and 10^{-5} (dotted line). Inset: Linear behavior of crossover frequency $\omega^*(\Delta p_b^J)$.

Our model features a second-order RP line meeting a first-order $B > 0$ line. Possible procedures for producing similar features in jammed systems include targeted selective pruning [21,27] or dividing bonds into those present in the marginal network at jamming and those added later followed by removal of the former and latter with respective probabilities p_a and p_b.

In this Letter, we introduced and analyzed, using effective medium theory and numerical simulations, a lattice model for jamming that captures the essential features of the jamming transition, which emerges as a critical end point in which a second-order rigidity percolation line meets a line in which there is a discontinuous jump in the bulk modulus from a nonrigid phase.

We thank Andrea Liu, Carl Goodrich and James Sethna for useful conversations. This work was supported in part by NSF MRSEC/DMR-1720530 (T. C. L. and O. S.), NSF DMR-1719490 (D. B. L.), and NSF DMR-1609051 (X. M.).

*dl778@cornell.edu
†tom@physics.upenn.edu

[1] A. J. Liu and S. R. Nagel, Annu. Rev. Condens. Matter Phys. **1**, 347 (2010).
[2] A. J. Liu and S. R. Nagel, Soft Matter **6**, 2869 (2010).
[3] S. Feng, M. F. Thorpe, and E. Garboczi, Phys. Rev. B **31**, 276 (1985).

[4] E. J. Garboczi and M. F. Thorpe, Phys. Rev. B **31**, 7276 (1985).
[5] R. J. Elliott, J. A. Krumhansl, and P. L. Leath, Rev. Mod. Phys. **46**, 465 (1974).
[6] D. B. Liarte, O. Stenull, X. M. Mao, and T. C. Lubensky, J. Phys. Condens. Matter **28**, 165402 (2016).
[7] J. C. Maxwell, Philos. Mag. **27**, 598 (1864).
[8] See Supplemental Material at http://link.aps.org/supplemental/10.1103/PhysRevLett.122.128006 for additional details of some of the main analytical and numerical results of this Letter.
[9] P. Chaikin and T. Lubensky, *Principles of Condensed Matter Physics* (Cambridge Press, Cambridge, England, 1995).
[10] L. M. Schwartz, S. Feng, M. F. Thorpe, and P. N. Sen, Phys. Rev. B **32**, 4607 (1985).
[11] D. J. Jacobs and M. F. Thorpe, Phys. Rev. Lett. **75**, 4051 (1995).
[12] M. Wyart, H. Liang, A. Kabla, and L. Mahadevan, Phys. Rev. Lett. **101**, 215501 (2008).
[13] M. Wyart, Europhys. Lett. **89**, 64001 (2010).
[14] X. M. Mao and T. C. Lubensky, Phys. Rev. E **83**, 011111 (2011).
[15] C. P. Broedersz, X. M. Mao, T. C. Lubensky, and F. C. MacKintosh, Nat. Phys. **7**, 983 (2011).
[16] X. M. Mao, O. Stenull, and T. C. Lubensky, Phys. Rev. E **87**, 042601 (2013).
[17] X. Mao, O. Stenull, and T. C. Lubensky, Phys. Rev. E **87**, 042602 (2013).
[18] G. During, E. Lerner, and M. Wyart, Soft Matter **9**, 146 (2013).
[19] M. G. Yucht, M. Sheinman, and C. P. Broedersz, Soft Matter **9**, 7000 (2013).
[20] C. P. Goodrich, A. J. Liu, and S. R. Nagel, Nat. Phys. **10**, 578 (2014).
[21] C. P. Goodrich, A. J. Liu, and S. R. Nagel, Phys. Rev. Lett. **114**, 225501 (2015).
[22] B. P. Tighe, Phys. Rev. Lett. **107**, 158303 (2011).
[23] L. E. Silbert, A. J. Liu, and S. R. Nagel, Phys. Rev. Lett. **95**, 098301 (2005).
[24] Our calculations show that the linear crossover from elasticity to isostaticity is akin to jamming *and* rigidity percolation. As shown in Supplemental Material [8], jamming and rigidity percolation can display different Debye behavior for the density of states at very low frequencies.
[25] C. R. Calladine, Int. J. Solids Struct. **14**, 161 (1978).
[26] C. P. Goodrich, A. J. Liu, and S. R. Nagel, Phys. Rev. Lett. **109**, 095704 (2012).
[27] W. G. Ellenbroek, V. F. Hagh, A. Kumar, M. F. Thorpe, and M. van Hecke, Phys. Rev. Lett. **114**, 135501 (2015).